Contact properties of a vdW heterostructure composed of penta-graphene and penta-BN_2 sheets

Kexian Zhao, Yaguang Guo, and Qian Wang

Citation: Journal of Applied Physics **124**, 165103 (2018); doi: 10.1063/1.5047539
View online: https://doi.org/10.1063/1.5047539
View Table of Contents: http://aip.scitation.org/toc/jap/124/16
Published by the American Institute of Physics

JOURNAL OF APPLIED PHYSICS **124**, 165103 (2018)

Contact properties of a vdW heterostructure composed of penta-graphene and penta-BN_2 sheets

Kexian Zhao,[1,2] Yaguang Guo,[1,2] and Qian Wang[1,2,a)]
[1]*Center for Applied Physics and Technology, Department of Materials Science and Engineering, College of Engineering, Peking University, Beijing 100871, China*
[2]*Key Laboratory of High Energy Density Physics Simulation, Ministry of Education, Beijing 100871, China*

(Received 8 July 2018; accepted 2 October 2018; published online 18 October 2018)

Recently, many efforts have been devoted to the study of 2D van der Waals (vdW) heterostructures because of their potential applications in new functional electronic and optoelectronic devices. Here, we propose a vdW heterostructure composed of the recently identified semiconducting penta-graphene (PG) and metallic penta-BN_2 (P-BN_2) monolayers. State-of-the-art theoretical calculations reveal that the intrinsic electronic properties of PG and P-BN_2 are well preserved in the heterostructure, an *n*-type Schottky barrier forms at the vertical interface between the two layers, and a negative band bending occurs at the lateral interface of the heterostructure and the PG monolayer. In addition, strain can be used to effectively tune the Schottky barrier. Both the Schottky barriers of electron and hole increase with stretching and decrease with compressing. More interestingly, the Schottky contact can be tuned from *n*-type to *p*-type when the interlayer distance between PG and P-BN_2 in the heterostructure is changed, showing a flexible controllability in device applications. *Published by AIP Publishing.* https://doi.org/10.1063/1.5047539

I. INTRODUCTION

Due to the fascinating properties and extraordinary applications of graphene,[1–4] two-dimensional (2D) carbon-based materials have attracted considerable attention in material science in recent years. A large number of new 2D carbon allotropes have been identified with a bunch of novel properties.[5–10] Among them, penta-graphene (PG),[10] composed of only pentagonal carbon rings, is particularly interesting as it possesses a negative Poisson's ratio, an ultra-high mechanical strength, and a quasi-direct band gap with the gap size close to that of traditional semiconductors, like GaN and ZnO, showing potentials for electronic device applications.

The unique geometry and novel properties of PG have stimulated a lot of study in the field of 2D materials, leading to the discovery of a new class of 2D materials entirely composed of pentagonal structural units explored theoretically[11–24] and experimentally.[25,26] On the other hand, it has been demonstrated that 2D materials can be used to construct van der Waals (vdW) heterostructures for electronic devices.[27–31] For example, PG was explored as a channel material contacting with graphene to form a vdW heterostructure.[32] It was found that there is a negative band bending at the lateral interface between the PG/G heterostructure and PG monolayer, leading to electron transfer from the heterostructure to the channel material PG. An n-type Schottky barrier (Φ_{SB}) is formed at the vertical interface of the PG and graphene layers, and the barrier height can be tuned by applying an external electric field or doping graphene with nitrogen atoms.

However, PG and graphene have very different lattice symmetry and parameters. Thus, special care is needed for dealing with the problem of their lattice mismatch in computational simulations. To avoid such a problem, here, instead of using graphene, we use the metallic penta-BN_2 sheet[19] as the metal electrode, because it is stable and metallic, and has the same lattice symmetry and nearly same lattice constants as those of PG. It would be interesting to see how different the performance of the heterostructure would be when its metallic electrode is changed from graphene to penta-BN_2. This motivates us to carry out the research on PG/P-BN_2 heterostructure.

II. COMPUTATIONAL METHODS

We study the structural and electronic properties of the heterostructure using density functional theory (DFT) as implemented in the Vienna *ab initio* simulation package (VASP).[33] We use the projector augmented wave (PAW) potential[34] to treat the ion-electron interactions with a kinetic energy cutoff of 400 eV, and the generalized gradient approximation (GGA)[35] with Perdew-Burke-Ernzerhof (PBE)[36] to describe the exchange and correlation interaction. Considering the special interaction between the two layers, the vdW correction DFT-D2[37] is applied to describe the vdW force. A vacuum space of 30 Å is used for eliminating the interaction between the adjacent cells in the vertical direction. All the atoms in the heterostructure are relaxed with a force convergence of 10^{-2} eV/Å and a total energy convergence of 10^{-4} eV. The first Brillouin zone is sampled by $15 \times 15 \times 1$ and $25 \times 25 \times 1$ k-point grids within the Monkhorst-Pack k-mesh[38] for the geometry optimization and electronic structure calculations, respectively.

III. RESULTS AND DISCUSSION

A. Geometric configurations of PG/P-BN_2 heterostructure

To construct a heterostructure of the PG and P-BN_2 monolayers, we first examine their lattice symmetries and

a)E-mail: qianwang2@pku.edu.cn

lattice parameters. The optimized lattice constants of PG and P-BN_2 are 3.64 and 3.63 Å, respectively, and both of them have p-42_1m symmetry. Obviously, their lattice constants match well, and the lattice mismatch is only 0.27%, as is the case with graphene/h-BN.[39] Therefore, the lattice stress is negligible when the primitive cells of the PG and P-BN_2 layers are vertically stacked together, while it needs to be minimized by means of constructing a large supercell in PG/graphene heterostructure.

Although 2D heterostructures can be constructed by stacking monolayers together, it is difficult to control the stacking configurations of heterostructures in experimental fabrication. Here, according to stacking misalignment (SM) rule,[40] we calculate a series of possible stacking patterns of PG/P-BN_2 heterostructure to find the lowest energy configuration. Based on AA stacking, we shift the PG layer along the x direction from 0 to 1/2 a with a step of 1/8 a; meanwhile, we shift this layer along the y direction with the same theory, where a is the optimized lattice constant of PG. The various stacking configurations are named $AA_{(m,\ n)}$, where m and n represent the shifting steps along x and y directions. We find that the most energetically favorable structure is $AA_{(0,\ 0)}$ (AA) stacking. Besides, we consider another stacking pattern into account named AA_r stacking which is constructed by setting the PG layer as the mirror of P-BN_2. We just demonstrate three patterns: AA, $AA_{(4,\ 4)}$ (AB) and AA_r which possess high symmetry as shown in Fig. 1. We show the relative total energy and find AA stacking has the lowest energy among them.

B. Stability and electronic properties of PG/P-BN_2 heterostructure

In the following, we focus our discussion only on the heterostructure with AA stacking configuration because of its lowest total energy. The binding energy between the two layers is defined as $E_b = {[E_{BN/C} - (E_{BN} + E_{PG})]}/{N}$, where $E_{BN/C}$ is the total energy of stacked heterostructure, E_{BN} and E_{PG} are the total energies of freestanding P-BN_2 and PG, respectively, and N is the total number of atoms in the P-BN_2 layer.

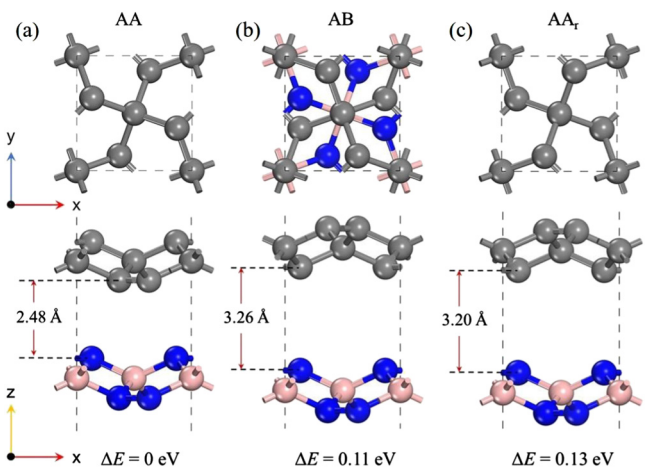

FIG. 1. Top and side views of the PG/P-BN_2 heterostructures: (a) AA stacking, (b) AB stacking, and (c) AA_r stacking. The relative energy ΔE and optimized interlayer distance are also provided here.

The binding energies of the heterostructure at different interlayer distances from 1.98 Å to 7.48 Å are calculated and plotted in Fig. 2(a). The results show that the binding energy between the two layers is −44.8 meV per carbon atom at the equilibrium interlayer distance of 2.48 Å, which is comparable with that of vdW structures like graphene/h-BN (−65 meV),[41,42] PG/G (−56 meV),[32] and graphite (−52 meV),[43] showing the feature of vdW interactions between the two layers.

Next, we carry out *ab initio* molecular dynamics (AIMD) simulations using a canonical ensemble to study the thermal stability of the PG/P-BN_2 heterostructure. To reduce the constraint of the periodic boundary condition, we apply the simulation with a $3 \times 3 \times 1$ supercell. We first perform the simulation at 300 K for 10 ps with a time step of 1 fs, and increase the temperature to 400 K, and then to 500 K, respectively. We find that the geometrical structure of PG/P-BN_2 heterostructure keeps well after 10 000 steps simulation, and the average value of the total potential energy remains nearly constant during the simulation even at the high temperature of 500 K. The variation of the total potential energy with respect to simulation time at 500 K is plotted in Fig. 2(b), confirming that the heterostructure is thermally stable at room temperature even up to 500 K.

To study the electronic properties of the PG/P-BN_2 heterostructure, we calculate the projected band structure, total density of states (DOS), and partial density of states (PDOS). The results are plotted in Fig. 2(c). In the band structure, the contributions from P-BN_2 and PG are colored in red and blue, respectively. We find that the original electronic properties of both PG and P-BN_2 are well preserved in this heterostructure, as compared to the results of previous studies,[10,19] because of the vdW interaction between the two monolayers. The contribution to the density of states near the Fermi level is mainly from N atom, which is relatively electron-rich as compared to B atom, while the valence and conduction bands are mainly contributed from the 3-coordinated carbon atoms in PG due to the more delocalized electronic feature.[44]

C. Device design and performance evaluation

Penta-graphene is semiconducting with a band gap of 3.25 eV and exhibits many other intriguing properties. Although it has not been synthesized yet, its Si analog (penta-Si) has already been fabricated.[25] It is reasonable to expect that with the advance of experimental synthesis together with the flexible bonding features of carbon, penta-graphene can be synthesized in the future. This motivates us to further explore the device applications of PG. We show two approaches that can effectively tune the Schottky barrier of PG-based metal-semiconductor junction, suggesting that PG has potential applications in electronic devices. These findings would further stimulate more experimental studies to synthesize PG and its applications.

For the potential application of the vdW heterostructure in electronic devices, the schematic view of a PG/P-BN_2 heterostructure-based field effect transistor (FET) is plotted in Fig. 3(a). There are two paths for charge carriers transferring from the electrode to the channel:[45] one is from the

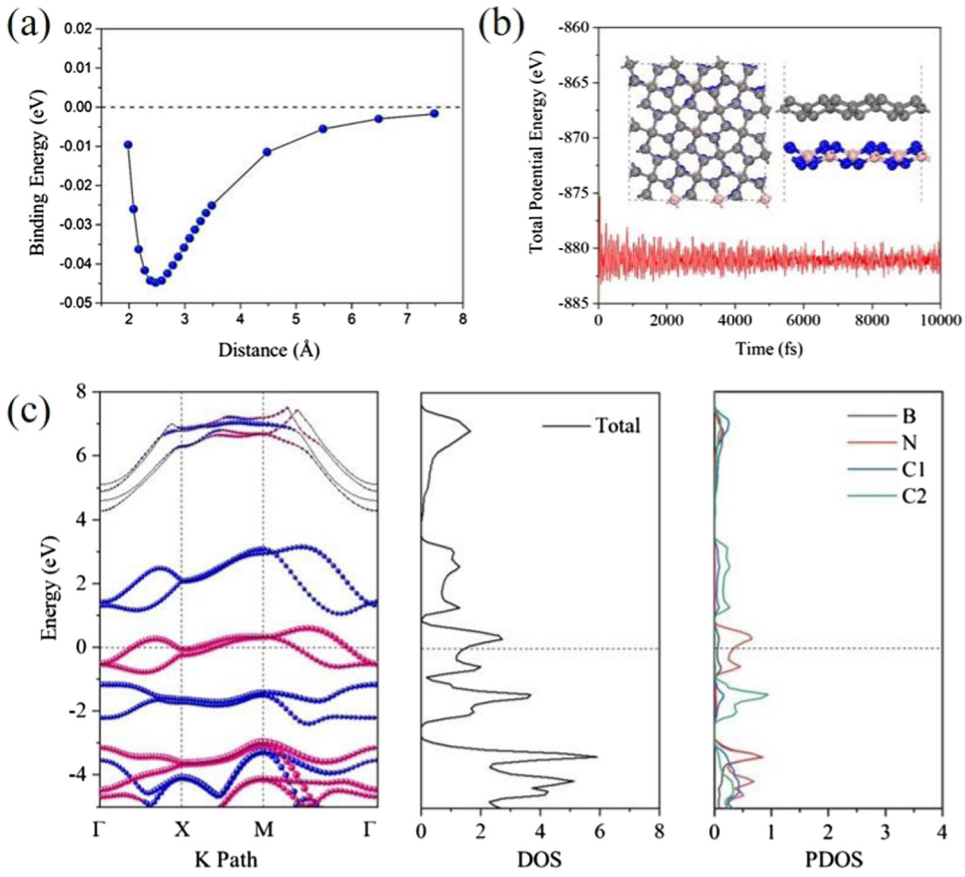

FIG. 2. (a) Variation of the binding energy with the interlayer distance between PG and P-BN_2. (b) Variation of the total potential energy of the heterostructure with simulation time during AIMD at 500 K. The insets are the top and side views of the geometrical structure at the end of the simulation. (c) The projected electronic band structures (the contributions from P-BN_2 and PG are colored in red and blue, respectively), and total and PDOS of the heterostructure.

metal to the semiconductor vertically with a Schottky barrier Φ_{SB}, and the other is from the heterostructure region to the freestanding channel material with a band bending ΔE_F. The Schottky barriers of electron and hole are defined as

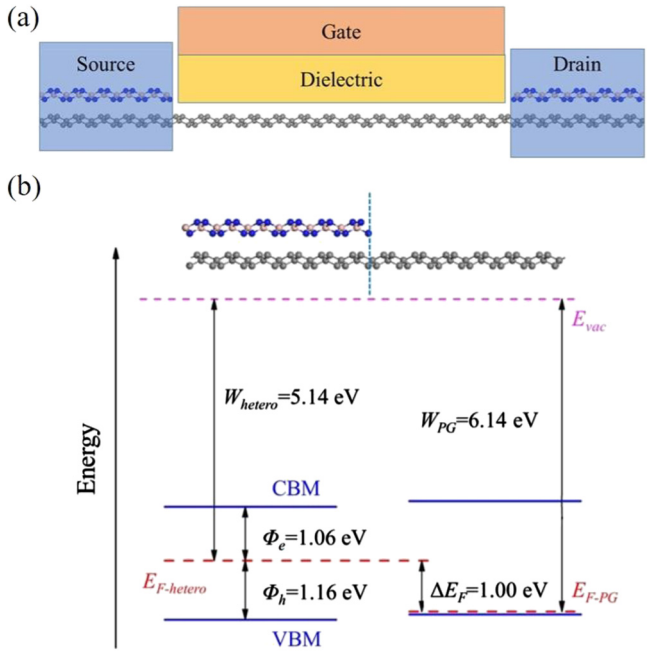

FIG. 3. (a) Schematic view of a P-BN_2/PG heterostructure based field-effect transistor. (b) Band alignment of the heterostructure and freestanding PG monolayer. E_{vac} is the vacuum level, W_{hetero} and W_{PG} are the work functions of the heterostructure and PG, and Φ_e and Φ_h represent electron and hole Schottky barriers, respectively.

$\Phi_e = E_{CBM} - E_F$, $\Phi_h = E_F - E_{VBM}$, where E_F is the Fermi level, and E_{CBM} and E_{VBM} are the energy levels of the conduction band minimum (CBM) and the valence band maximum (VBM) of PG in the heterostructure, respectively. The band bending ΔE_F is defined by the difference of the Fermi levels of the heterostructure ($E_{F\text{-}hetero}$) and PG ($E_{F\text{-}PG}$).

To show the charge transfer in the heterostructure-based FET, the band alignments of the vdW heterostructure and freestanding PG monolayer are plotted in Fig. 3(b). The left part is for the PG/P-BN_2 vdW heterostructure, and the right part is for the PG monolayer. The Schottky barriers for electron (Φ_e) and hole (Φ_h) are calculated to be 1.06 and 1.16 eV, respectively, while the band bending (ΔE_F) is −1.00 eV, indicating that electrons can transfer from the heterostructure region to the channel region (the PG monolayer), thus leading to an *n*-type channel similar to the situation in PG/G heterostructure.[32]

In order to visualize the charge redistribution in the vdW heterostructure, the plane average charge density difference and the 3D charge density difference are plotted in Figs. 4(a) and 4(b), respectively. The charge density difference is calculated by using the formula: $\Delta\rho = \rho_H - \rho_{PG} - \rho_{BN}$, where ρ_H, ρ_{PG}, and ρ_{BN} represent the charge density of the heterostructure, PG, and P-BN_2, respectively. From Fig. 4(a), one can see that the charge redistribution is significant at the interface of the heterostructure. Figure 4(b) shows that electrons mainly accumulate on the lowest carbon atoms in PG, and the topmost nitrogen atoms in P-BN_2, unlike the case of graphene/h-BN heterostructure in which the electrons

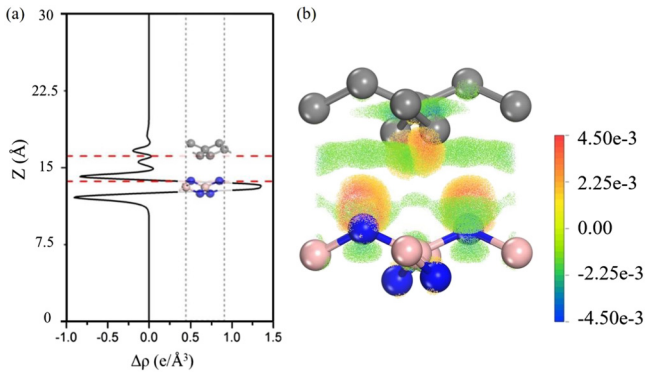

FIG. 4. (a) Plane-average charge density difference of the heterostructure. The inset is the geometrical structure, and the red dashed lines represent the positions of the lowest carbon atoms in PG and the topmost nitrogen atoms in P-BN_2. (b) 3D charge density difference of the heterostructure. Blue and red isosurfaces represent depletion and accumulation of charge, respectively.

accumulate along the C-C and B-N bonds.[46] It is obvious that the charge redistribution is asymmetric between the two layers, resulting in the formation of the interface dipole moment leading to the inter-layer vdW interaction.

D. Modulation of Schottky barrier

Strain is widely used to tune the electronic properties of heterostructures.[31,47–50] Due to the outstanding mechanical properties of PG and P-BN_2,[10,19] we respectively apply uniaxial and biaxial strains in the x-y-plane varying from −5% to 5% to tune the electronic structures of the heterostructure, as shown in Fig. 5. The strain ε is defined as $\varepsilon = (a - a_0)/a_0$, where a and a_0 are the lattice constants with and without stain, respectively. Figure 5(a) shows the effect of biaxial strain on the band structure of the heterostructure, where the contribution from PG is colored in blue, and the red and black dots represent the VBM and the CBM, respectively. We find that the VBM of PG in heterostructure lies at the path of Γ to X when stretching, which is same as the original heterostructure without strain, but locates at the Γ point with compressing from 0% to −3%, and at the M point with compression larger than −4%, whereas the CBM is located at the path of M to Γ all the time. To explain the phenomena, we study the effects of applying strains on monolayer pentagraphene whose VBM has several sudden changes with the increase of strain, which are in good agreement with previous

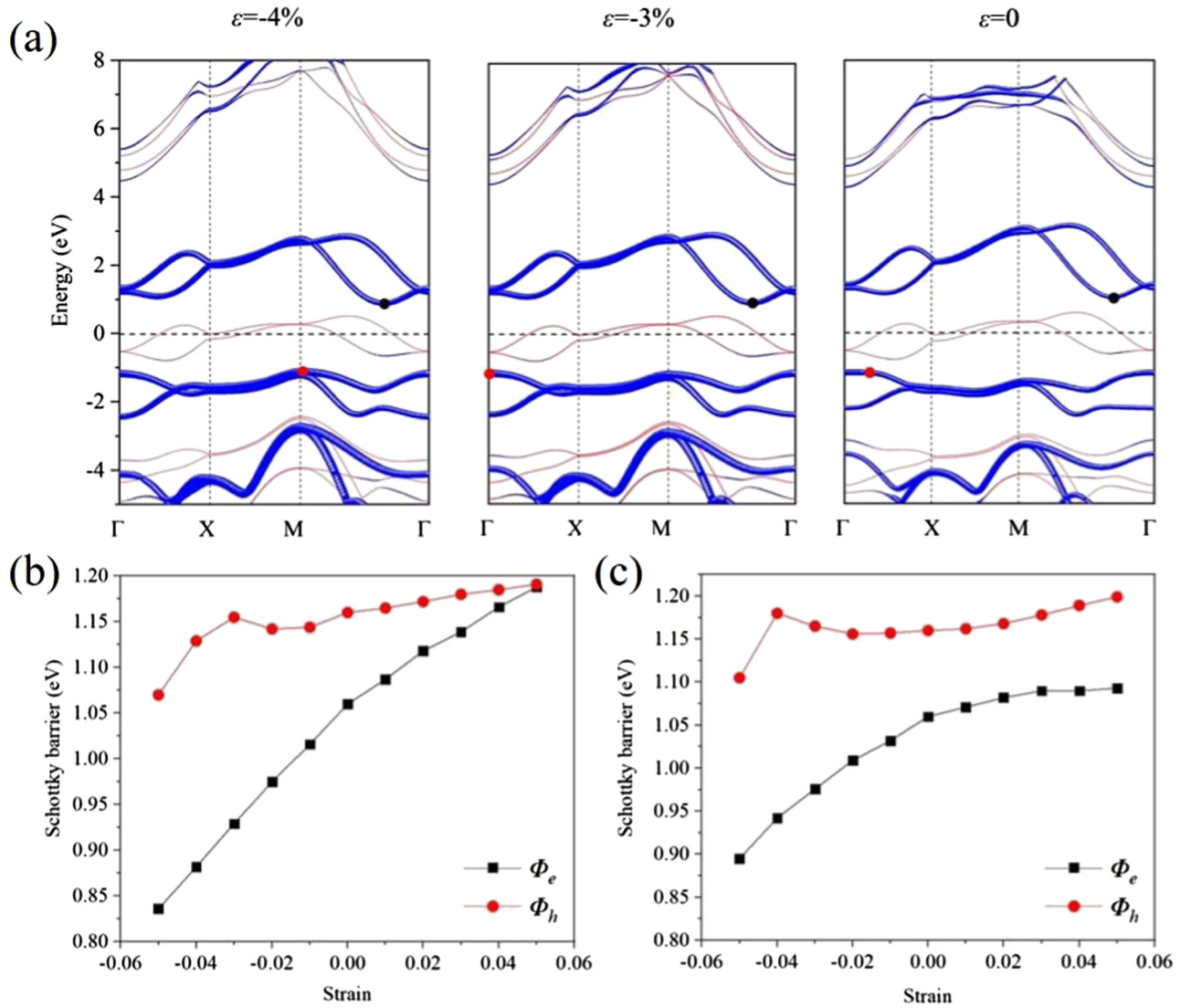

FIG. 5. (a) Band structures under different biaxial strains. Variations of the Schottky barrier with (b) biaxial and (c) uniaxial strains, respectively.

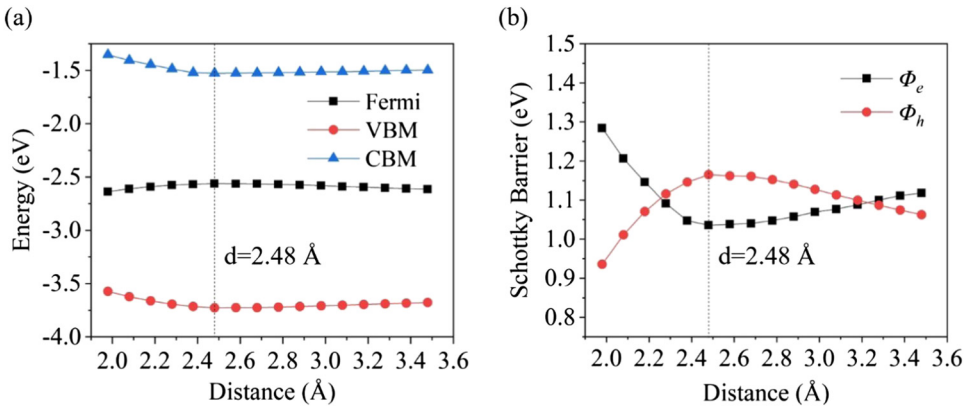

FIG. 6. Variation of (a) the energy level of Fermi, VBM, and CBM, and (b) the Schottky barrier heights with the interlayer distance between PG and P-BN_2.

work[51] and conforming to the results in heterostructure because of the vdW interaction. Under tensile strain, the CBM of PG shifts upward slightly, while both the Fermi level and VBM move downward, and the latter drops off faster than the former. Therefore, both Φ_e and Φ_h exhibit an increasing trend, and Φ_e is more sensitive to the strain. On the contrary, when compressing the heterostructure, the Fermi level and VBM move upward, leading to a decreasing trend of Φ_e. We also note that Φ_h decreases overall with slight oscillations under the compressing strain in the range from 0% to −5%, as shown in Figs. 5(b) and 5(c).

Besides the in-plane strain, another way can be used to tune the Schottky barrier of the vdW heterostructure. We change the interlayer distance between the PG and P-BN_2 monolayers from 1.98 to 3.48 Å and find that the Fermi level decreases when the interlayer distance deviates from its equilibrium position of 2.48 Å. While both the VBM and CBM show opposing trends, the energy level increases when the interlayer distance is enlarged or reduced [see Fig. 6(a)]. Therefore, Φ_h and Φ_e, respectively, reach the maximum and minimum values at the equilibrium interlayer distance. Moreover, the variations of Schottky barrier heights for electrons and holes with the interlayer distance are plotted in Fig. 6(b). A *p*-type heterostructure forms when the distance is in the range of 1.98 to 2.28 Å because of $\Phi_h < \Phi_e$, while it becomes an *n*-type contact when the distance is in the range of 2.28 to 3.18 Å due to $\Phi_e < \Phi_h$, and it returns to a *p*-type when the distance is larger than 3.18 Å. In short, the interlayer distance can effectively tune the Schottky barrier height, realizing the transformation of Schottky barrier from *n*-type to *p*-type.

IV. CONCLUSIONS

In summary, we have studied a vdW heterostructure composed of the PG and P-BN_2 monolayers by using DFT with a vdW correction functional of DFT-D2. The most energetically favorable structure is found to be an AA stacking pattern with a lattice mismatch less than 0.3%. Different from the previously reported PG/graphene heterostructure, PG/P-BN_2 heterostructure has less lattice strain and is thermally more stable, and can withstand a temperature up to 500 K. Due to the outstanding mechanical properties of PG and P-BN_2, the Schottky barriers of electron and hole (Φ_e and Φ_h) can be effectively tuned by applying uniaxial and biaxial strains, where Φ_e shows an increasing tendency when external strain changes from −5% to 5%, and Φ_h is largely affected by the CBM of PG when compressing the heterostructure. In addition, the Schottky barrier can be tuned from *n*-type to *p*-type by varying the interlayer distance between the PG and P-BN_2 monolayers, showing a flexible modulation of the contact properties in the PG/P-BN_2 heterostructure. Our study provides information on the design and fabrication of PG-based electronic devices.

ACKNOWLEDGMENTS

This work was partially supported by grants from the National Key Research and Development Program of China (No. 2016YFE0127300), the National Natural Science Foundation of China (Nos. NSFC-51471004 and NSFC-21773004), and supported by the High Performance Computing Platform of Peking University, China.

[1]K. S. Novoselov, A. K. Geim, S. V. Morozov, D. Jiang, M. I. Katsnelson, I. V. Grigorieva, S. V. Dubonos, and A. A. Firsov, Nature **438**, 197 (2005).
[2]V. P. Gusynin and S. G. Sharapov, Phys. Rev. Lett. **95**, 146801 (2005).
[3]K. S. Novoselov, Z. Jiang, Y. Zhang, S. V. Morozov, H. L. Stormer, U. Zeitler, J. C. Maan, G. S. Boebinger, P. Kim, and A. K. Geim, Science **315**, 1379 (2007).
[4]J. H. Chen, C. Jang, S. D. Xiao, M. Ishigami, and M. S. Fuhrer, Nat. Nanotechnol. **3**, 206 (2008).
[5]Y. Liu, G. Wang, Q. Huang, L. Guo, and X. Chen, Phys. Rev. Lett. **108**, 225505 (2012).
[6]Y. Li, L. Xu, H. Liu, and Y. Li, Chem. Soc. Rev. **3**, 2572 (2014).
[7]Z. Wang, X. F. Zhou, X. Zhang, Q. Zhu, H. Dong, M. Zhao, and A. R. Oganov, Nano Lett. **15**, 6182 (2015).
[8]A. R. Puigdollers, G. Alonso, and P. Gamallo, Carbon **96**, 879 (2016).
[9]X. Li, Q. Wang, and P. Jena, J. Phys. Chem. Lett. **8**, 3234 (2017).
[10]S. H. Zhang, J. Zhou, Q. Wang, X. S. Chen, Y. Kawazoe, and P. Jena, Proc. Natl. Acad. Sci. U.S.A. **112**, 2372 (2015).
[11]A. Lopez-Bezanilla and P. B. Littlewood, J. Phys. Chem. C **119**, 19469 (2015).
[12]M. Yagmurcukardes, H. Sahin, J. Kang, E. Torun, F. M. Peeters, and R. T. Senger, J. Appl. Phys. **118**, 104303 (2015).
[13]X. Li, Y. Dai, M. Li, W. Wei, and B. Huang, J. Mater. Chem. A **3**, 24055 (2015).
[14]C. Zhang, S. Zhang, and Q. Wang, Sci. Rep. **6**, 29531 (2016).
[15]H. Liu, G. Qin, Y. Lin, and M. Hu, Nano Lett. **16**, 3831 (2016).
[16]Y. Ding and Y. Wang, J. Mater. Chem. C **3**, 11341 (2015).
[17]Y. Wang, Y. Li, and Z. Chen, J. Mater. Chem. C **3**, 9603 (2015).
[18]Y. Aierken, O. Leenaerts, and F. M. Peeters, Phys. Chem. Chem. Phys. **18**, 18486 (2016).
[19]J. Li, X. Fan, Y. Wei, and G. Chen, Sci. Rep. **6**, 31840 (2016).
[20]S. Zhang, J. Zhou, Q. Wang, and P. Jena, J. Phys. Chem. C **120**, 3993 (2016).

[21]J. Li, X. Fan, Y. Wei, H. Liu, S. Li, P. Zhao, and G. Chen, Sci. Rep. **6**, 33060 (2016).
[22]J. Chen, G. Schusteritsch, C. J. Pickard, C. G. Salzmann, and A. Michaelides, Phys. Rev. Lett. **116**, 025501 (2016).
[23]Y. Ma, L. Kou, X. Li, Y. Dai, and T. Heine, NPG Asia Mater. **8**, e264 (2016).
[24]S. Liu, B. Liu, X. Shi, J. Lv, S. Niu, M. Yao, Q. Li, R. Liu, T. Cui, and B. Liu, Sci. Rep. **7**, 2404 (2017).
[25]J. I. Cerda, J. Slawinska, G. Le Lay, A. C. Marele, J. M. Gomez-Rodriguez, and M. E. Davila, Nat. Commun. **7**, 13076 (2016).
[26]A. D. Oyedele, S. Yang, L. Liang, A. A. Puretzky, K. Wang, J. Zhang, P. Yu, P. R. Pudasaini, A. W. Ghosh, Z. Liu, C. M. Rouleau, B. G. Sumpter, M. F. Chisholm, W. Zhou, P. D. Rack, D. B. Geohegan, and K. Xiao, J. Am. Chem. Soc. **139**, 14090 (2017).
[27]L. Britnell, R. V. Gorbachev, R. Jalil, B. D. Belle, F. Schedin, A. Mishchenko, T. Georgiou, M. I. Katsnelson, L. Eaves, S. V. Morozov, N. M. R. Peres, J. Leist, A. K. Geim, K. S. Novoselov, and L. A. Ponomarenko, Science **335**, 947 (2012).
[28]L. Yu, Y. H. Lee, X. Ling, E. J. Santos, Y. C. Shin, Y. Lin, M. Dubey, E. Kaxiras, J. Kong, H. Wang, and T. Palacios, Nano Lett. **14**, 3055 (2014).
[29]C. J. Shih, Q. H. Wang, Y. Son, Z. Jin, D. Blankschtein, and M. S. Strano, ACS Nano **8**, 5790 (2014).
[30]L. Huang and J. Li, Appl. Phys. Lett. **108**, 083101 (2016).
[31]L. Huang, Y. Li, Z. Wei, and J. Li, Sci. Rep. **5**, 16448 (2015).
[32]Y. G. Guo, F. Q. Wang, and Q. Wang, Appl. Phys. Lett. **111**, 073503 (2017).
[33]G. Kresse and J. Furthmuller, Phys. Rev. B **54**, 11169 (1996).
[34]G. Kresse and D. Joubert, Phys. Rev. B **59**, 1758 (1999).
[35]P. E. Blochl, Phys. Rev. B **50**, 17953 (1994).
[36]J. P. Perdew, K. Burke, and M. Ernzerhof, Phys. Rev. Lett. **77**, 3865 (1996).
[37]H. J. Monkhorst and J. D. Pack, Phys. Rev. B **13**, 5188 (1976).
[38]S. Grimme, J. Comput Chem. **27**, 1787 (2006).
[39]K. S. Novoselov, A. Mishchenko, A. Carvalho, and A. H. Castro Neto, Science **353**, aac9439 (2016).
[40]Z. G. Yu and Y.-W. Zhang, J. Appl. Phys. **118**, 165706 (2015).
[41]G. Graziano, J. Klimes, F. Fernandez-Alonso, and A. Michaelides, J. Phys. Condens. Matter **24**, 424216 (2012).
[42]B. Sachs, T. O. Wehling, M. I. Katsnelson, and A. I. Lichtenstein, Phys. Rev. B **84**, 195414 (2011).
[43]R. Zacharia, H. Ulbricht, and T. Hertel, Phys. Rev. B **69**, 155406 (2004).
[44]G. R. Berdiyorov and M. E. A. Madjet, RSC Adv. **6**, 50867 (2016).
[45]J. H. Kang, W. Liu, and K. Banerjee, Appl. Phys. Lett. **104**, 173105 (2014).
[46]A. M. Ukpong, Comput. Condens. Matter **2**, 1 (2015).
[47]N. Lu, H. Guo, L. Li, J. Dai, L. Wang, W. N. Mei, X. Wu, and X. C. Zeng, Nanoscale **6**, 2879 (2014).
[48]X. He, H. Li, Z. Zhu, Z. Dai, Y. Yang, P. Yang, Q. Zhang, P. Li, U. Schwingenschlogl, and X. Zhang, Appl. Phys. Lett. **109**, 173105 (2016).
[49]W. Yu, Z. Zhu, S. Zhang, X. Cai, X. Wang, C. Y. Niu, and W. B. Zhang, Appl. Phys. Lett. **109**, 103104 (2016).
[50]G. H. Lee, Y. J. Yu, X. Cui, N. Petrone, C. H. Lee, M. S. Choi, D. Y. Lee, C. Lee, W. J. Yoo, K. Watanabe, T. Taniguchi, C. Nuckolls, P. Kim, and J. Hone, ACS Nano **7**, 7931 (2013).
[51]M. Shahrokhi, Optik **136**, 205 (2017).